JOURNAL OF Materials CHEMISTRY

Isomorphous substitution of ruthenium in MFI framework using the oxo-anions ruthenate(VI) and perruthenate(VII)

Kay Latham,[a] David Thompsett,[b] Craig D. Williams*[c] and Catherine I. Round[c]

[a]*Department of Applied Chemistry, RMIT University, City Campus, Melbourne 3001, Victoria, Australia*
[b]*Johnson Matthey, Technology Centre, Blount's Court, Sonning Common, Reading, UK RG4 9NH*
[c]*School of Applied Sciences, University of Wolverhampton, Wolverhampton, UK WV1 1SBC. Williams@wlv.ac.uk*

Received 24th January 2000, Accepted 3rd February 2000

The oxo-anions: ruthenate(VI) and perruthenate(VII), as primary sources of ruthenium, have been investigated in the hydrothermal synthesis of zeolite ZSM-5. Crystalline material with ruthenium incorporated into lattice sites was isolated from starting gels containing up to 0.1 mole fraction Ru_2O_3/SiO_2. There are no previous reports of the isomorphous replacement of aluminium by ruthenium in MFI-type zeolites. X-Ray diffraction, infra-red spectroscopy, chemical analysis, electron microscopy, and X-ray photoemission spectroscopy (XPS) all provide evidence for the presence of framework ruthenium. The development of new IR absorption bands in the asymmetric and symmetric Si–O–T stretching region, and the shift to lower wavenumbers is accompanied by an increase in the interplanar spacings and unit-cell dimensions with increased Al replacement. A change in morphology is also observed.

Introduction

The isomorphous replacement of Al or Si in the zeolite framework by heteroatoms produces new materials with significantly modified physico/chemical and catalytic properties.[1] These materials have the potential to carry out petrochemical and/or organic reactions.[2] The incorporation of ruthenium into zeolites has been recently reviewed.[3] The Ru^{3+} ion has a larger ionic radius (0.69 Å) than Al^{3+} (0.57 Å) and, like iron (preceding member of Group VIII), it has a tendency to form insoluble hydroxides in a basic environment and an ability to change oxidation state.

We report the synthesis of crystalline MFI zeolite in which up to twice the amount of Al_2O_3 has been replaced by Ru_2O_3 in the reaction gel. This has been achieved using potassium ruthenate(VI), K_2RuO_4, and tetra-*n*-propylammonium perruthenate(VII), $(Pr_4N)RuO_4$. The use of ruthenium salts and complexes in impregnation *i.e.* secondary synthesis and surface treatment has been widely documented,[4,5] but it would appear that the use of basic, tetrahedral ruthenium species, RuO_4^{2-} and RuO_4^{-}, as primary reagents in zeolite synthesis, is unexplored. It was anticipated that the RuO_4^{2-} and RuO_4^{-} ions, which are moderately stable in strongly alkaline media and have tetrahedral geometry (isostructural to $Al(OH)_4^{-}$), would encourage the nucleation of zeolite species. Tetra-*n*-propylammonium perruthenate(VII) is more widely known in organic synthesis, where it is used as a selective catalytic oxidant.[6]

Experimental

Materials

The synthesis of ruthoaluminosilicate MFI was carried out at 150 ± 1 °C in sealed stainless steel autoclaves (500 cm^3). The raw materials used were: potassium ruthenate [K_2RuO_4], prepared by fusing a mixture of potassium hydroxide, potassium nitrate and commercial ruthenium trichloride in a nickel crucible at red heat;[7] tetra-*n*-propylammonium perruthenate [$(Pr_4N)RuO_4$] (97+%, Lancaster Synthesis); fine aluminium powder (GPR, BDH), fumed silica (98% CAB-O-SIL M5, BDH Scintran); potassium hydroxide pellets (GPR, Scientific and Chemical Supplies Ltd., Bilston, West Midlands); tetrapropylammonium bromide (98+%, Fluka Chemika); and deionised water.

Synthesis

The replacement of aluminium in crystalline zeolite MFI by ruthenium was attempted systematically. The starting molar compositions[8] were: $(311-x)K_2O{\cdot}xK_2RuO_4{\cdot}(160-0.5x)Al_2O_3{\cdot}2956SiO_2{\cdot}667TPABr{\cdot}148400H_2O$ (where $x = 0$, 32, 64, 320 and 640); and $311K_2O{\cdot}x[(Pr_4N)RuO_4]{\cdot}(160-0.5x)Al_2O_3{\cdot}2956SiO_2{\cdot}(667-x)TPABr{\cdot}148400H_2O$ (where $x = 320$). The reagent amounts for each experiment are given in Table 1.

(Al)-ZSM-5 and ruthenate(VI)-containing gels were prepared as follows. The silica (20.20 g, CAB-O-SIL M-5), and aluminium powder (0.89 g) were weighed out, separately. Potassium hydroxide (3.56 g) was added to the aluminium, and following the addition of water (100 cm^3), the mixture was left for 20 minutes to allow dissolution. Water (167 cm^3) was added to the silica source, followed by solid potassium ruthenate (0.89 g), stirred thoroughly and allowed to age for 20 minutes. The alkaline aluminate solution was then added to the silica/ruthenate solution, and aged for 5 minutes before addition of the template solution (20.20 g TPABr, 37.26 cm^3 water). The resulting orange gel was electrically mixed for 30 seconds and transferred to the steel autoclave. Periodically, samples were removed and cooled, and solid products were separated from the mother liquor by Buchner filtration. The samples were then washed with deionised water (3×50 cm^3) and heated overnight at 40 ± 1 °C in a drying oven.

Owing to the oxidative nature of the perruthenate complex, the order of addition of reagents was modified. Dry perruthenate solid was added to dry TPABr, followed by the addition of water. This solution was then added to a mixture of silica and water, and allowed to age for 20 minutes. The potassium hydroxide mineralising solution was then added, the

Table 1 Amount of reagents used in syntheses

Reagent	Amounts of reagents/g					
	$x=0.0$	$x=32$	$x=64$	$x=320$	$x=320$ (Ru(VII))	$x=640$
KOH	3.98	3.56	5.37	—	3.96	—
Al	0.98	0.89	0.44	—	—	—
K_2RuO_4	—	0.89	1.76	8.77	—	17.11
$(Pr_4N)RuO_4$	—	—	—	—	12.74	—
SiO_2	20.24	20.20	20.07	20.00	20.11	19.51
TPABr	20.23	20.20	20.08	20.01	10.48	19.52
H_2O	304.57	304.26	302.28	301.22	302.71	293.86
Total	350.00	350.00	350.00	350.00	350.00	350.00

resulting gel stirred, aged for 5 minutes, and mixed electronically for 30 seconds. All other aspects of the synthesis were as (Al)-ZSM-5 and ruthenate(VI) gels.

Instrumentation

Solid products were characterised using conventional techniques. The crystallinity of materials was determined from XRD patterns recorded on a Philips 1710 X-ray diffractometer using Cu-Kα radiation. The samples were compared by computerised on-line isotypical search to the ICDD standard 38-195 [H–Al_2O_3–SiO_2]. The size, shape and morphology of the zeolite crystals were examined using a scanning electron microscope (Philips 515) after coating with gold-evaporated film on an aluminium peg. The framework IR spectra reported are for hydrated zeolites supported in alkali halide wafers. The samples (0.5 mg) were uniformly mixed with 200 mg dry KBr (BDH SpectrosoL) and ground by hand in a pestle and mortar for 5 minutes. The mixture was then pressed at 9 tonnes to give a transparent fused halide window (12.5 mm diameter). Spectra were recorded in air at room temperature on a Nicolet Impact 404 FTIR spectrophotometer. Thermogravimetric analysis was performed on a Mettler TG50 thermobalance/Mettler TA3000 processor in nitrogen, air and oxygen at a heating rate of 20 K min^{-1} using approximately 15 mg of sample. Chemical composition was determined by Energy Dispersive X-Ray (EDX) analysis (CamScan SV2) of the uncoated sample on a carbon peg.

Four samples were analysed using XPS spectroscopy: $x=64$ (20% mole fraction Ru_2O_3 as K_2RuO_4); $x=320$ (100% mole fraction Ru_2O_3 as K_2RuO_4); $x=640$ (200% mole fraction Ru_2O_3 as K_2RuO_4); and RuO_2. The samples were mounted on the sample stubs using double-sided adhesive tape and analysed using Mg-Kα radiation at 195 W with 7.5 mm slits and 160, 80 and 40 eV pass energies. The binding energies were related to C1s at 284.8 eV and the quantitation was performed using intensity data and a linear background subtraction procedure.

Results and discussion

Fully crystalline MFI zeolites were obtained from systems containing up to $x=640$ Ru_2O_3. The products from systems containing 0 and 64 mole fractions were crystalline white solids. Materials with $x>320$ were grey in colour but showed good pattern matching to ICDD [38-195] by X-ray diffraction.

The kinetics of crystallisation were followed by XRD measurements on the washed, dry solids. The $x=32$ Ru-ZSM-5 began to crystallise after 50 hours and the crystallisation process was complete after 10 days (Fig. 1). This was similar to the kinetics for pure (Al)-ZSM-5 and the $x=64$, 320, and 640 Ru-ZSM-5 samples prepared using potassium ruthenate(VI). The $x=320$ Ru-ZSM-5 prepared using tetra-*n*-propylammonium perruthenate(VII) was fully crystalline at 47 hours.

It was noted that the XRD reflections for ruthenium-substituted samples were shifted to higher *d* values compared to

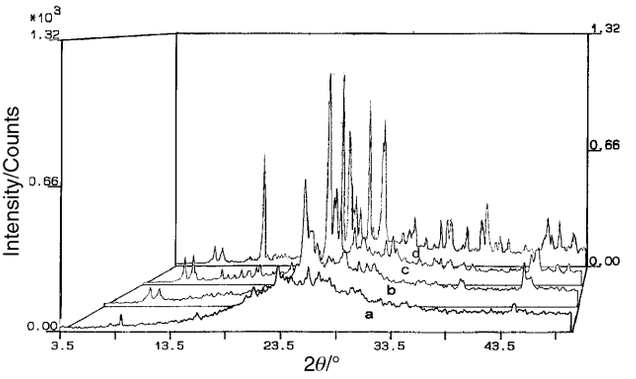

Fig. 1 A 3-dimensional comparison of XRD spectra of samples from an $x=32$ ruthenium-substituted ZSM-5 gel after a) 50 hours, b) 5 days, c) 7 days and d) 10 days at 150 °C.

Al-ZSM-5. The positions for *hkl*(150), the most prominent peak, for each crystalline zeolite are shown in Fig. 2. This shift was accompanied by changes in the unit-cell parameters: cell dimensions (*a*, *b*, *c*), and a decrease in the *a*/*b* ratio with increased Al^{3+} replacement (Table 2). These changes are significant evidence for framework incorporation of ruthenium.

SEM micrographs of the Al-MFI and the ruthenium-containing samples indicate good quality crystals of even distribution and a little amorphous material. The crystals were generally 18 × 8 μm in size. A distinct change in morphology is also observed on increasing the ruthenium content (Fig. 3). The crystals can be described as 'interpenetrated twin barrel' shaped, cylindrical with a length : diameter ratio of ~0.5. The Al-MFI samples are twinned with a series of steps or terraces. The ruthenium-substituted crystals have twins of increasing

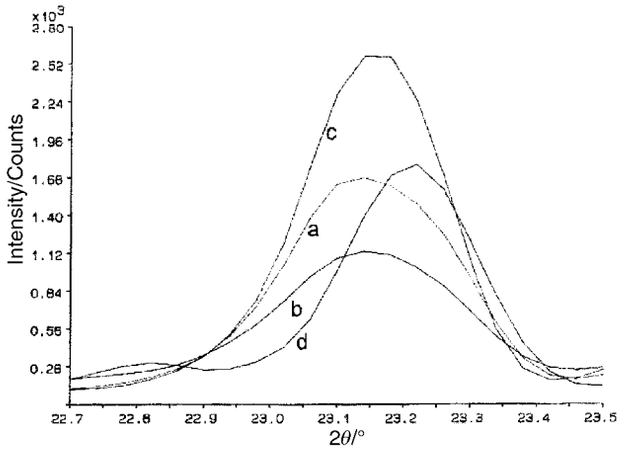

Fig. 2 Graph to show the change in position of the main XRD reflection (*hkl* 150) with increasing ruthenium substitution: a) (Al)-ZSM-5; and $x=$ b) 32, c) 320, d) 640 Ru-ZSM-5.

Table 2 Comparison of cell dimensions (*a*, *b*, *c*), *a*/*b* ratio and unit cell volumes for MFI and ruthenium substituted samples (space group *Pnma*)

x	*a*/Å	*b*/Å	*c*/Å	*a*/*b*	Unit cell/Å^3
0	20.03308	19.88637	13.39121	1.007	5334.85
32	20.52282	19.95959	13.30740	1.028	5451.08
64	20.18008	19.96503	13.45141	1.011	5419.51
320	19.95115	20.04782	13.40688	0.995	5362.43
320 (Ru(VII))	19.91100	20.06200	13.53100	0.992	5405.01
640	19.86146	20.15629	13.36687	0.985	5351.19

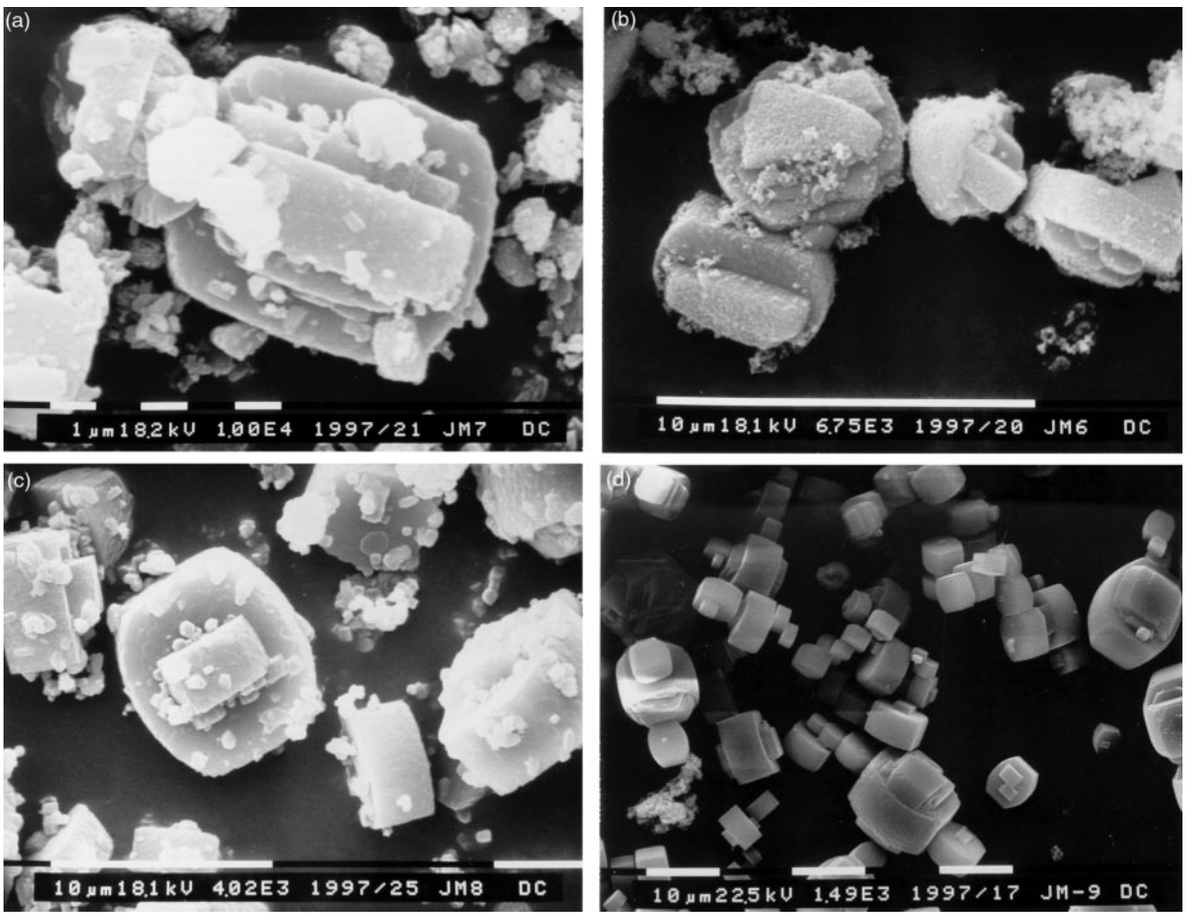

Fig. 3 SEM micrographs of a) (Al)-ZSM-5; and $x=$ b) 32 Ru(Al)-ZSM-5, c) 320 Ru-ZSM-5, and d) 640 Ru-ZSM-5; showing increased surface flatness with increased ruthenium substitution.

flatness and become more rounded with increased aluminium replacement (Fig. 3a–d). This morphological effect has also been reported by Verduijn[9] for the incorporation of increasing levels of iron in aluminosilicate K-LTL. A general decrease in crystal size on increased iron substitution was also recorded.

The IR spectra of zeolite MFI and its ruthenium-containing analogues closely agree with the literature.[10] The characteristic spectra (2000–400 cm^{-1}) are shown in Fig. 4. Evidence for framework siting of Ru atoms is suggested by the appearance of a new band (shoulder) at approximately 990 cm^{-1}, which is absent in the IR spectrum of pure (Al)-ZSM-5. The relative intensity of this shoulder increases with increasing ruthenium content in the gel (Fig. 4a–d). Slight shifts are also observed in the Si–O–T asymmetric ($\sim$500 cm^{-1}) and symmetric ($\sim$800 cm^{-1}) stretching vibrations and the T–O bend ($\sim$1100 cm^{-1}). The splitting observed for $x=320$ and 640 ruthenium-substituted samples may indicate a change in bond angle.

All samples were calcined in an air stream to a temperature of 550 °C, and held under these conditions for 16 hours. The Ru-ZSM-5 (Ru(VI)) showed excellent phase stability, at the lower substitution levels ($x \geqslant 32$), and only very slight traces of ruthenium(IV) oxide (RuO_2) were observed in the $x=320$ and

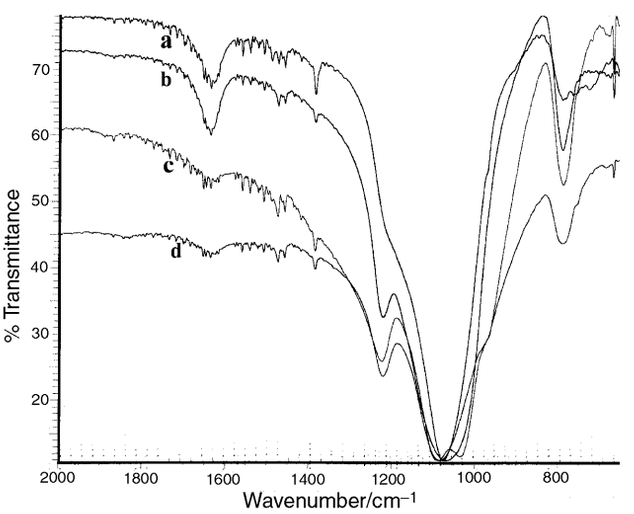

Fig. 4 IR bands exhibited by a) pure (Al)-ZSM-5; and $x=$ b) 32, c) 320 and d) 640 ruthenium-containing ZSM-5 in the region 2000–400 cm^{-1}.

640 Ru-substituted samples. A modification to the calcination procedure, by heating the sample to 550 °C at a rate of 10 °C min^{-1} under nitrogen, resulted in clean, calcined ZSM-5.

The $x = 320$ (Ru)ZSM-5 prepared using TPA perruthenate-(VII) showed poor thermal stability. Post calcination, in air or nitrogen, a considerable loss of crystallinity was observed, and the sample became very dark grey in appearance, indicating the presence of appreciable amounts of occluded and surface RuO_2. This suggests that if Ru is taken into the framework, it is only loosely held. There are many discussions in the literature regarding the siting of aluminium/heteroatoms within ZSM-5 crystals—ranging from moderate disorder[11] to precise siting at the junctions of the linear and sinusoidal channels, *i.e.* close to the TPA^+ counterions.[12] It may be that the TPA–Ru bond is somewhat 'stronger' than the K–Ru bond and thus TPA perruthenate(VII) is less willing to release ruthenium for coordination within the zeolite framework, resulting in a weak association which readily collapses on heating to give finely dispersed ruthenium(VI) oxide within the annealed silicate.

Thermal characteristics were more closely examined by thermogravimetric analysis. The DTG trace for pure (Al)-ZSM-5 (Si/Al = 9) heated in flowing nitrogen is shown in Fig. 5a. After a marked water loss (< 200 °C), corresponding to the amount of hydrated potassium ions present, thermal analysis revealed a single, well-defined and relatively symmetrical mass loss with a peak minimum at 460 °C. This peak is associated with the endothermic decomposition of charge-compensating TPA^+ ions. The introduction of ruthenium into the reaction gel resulted in considerable changes to the thermal profile. The profiles for $x = 64$, 320 and 640 Ru-ZSM-5 (Ru(VI)), and the $x = 320$ Ru-ZSM-5 (Ru(VII)) are shown in (Fig. 5b,c,d,e). Overall, the mass loss below 200 °C decreased, and the 350–550 °C region became more asymmetric and complex, with the temperature for major 'template' loss decreasing, on increased ruthenium substitution (Table 3). The reduced water loss is mirrored by the decreasing K^+ content in the ruthenium-substituted samples. It may also

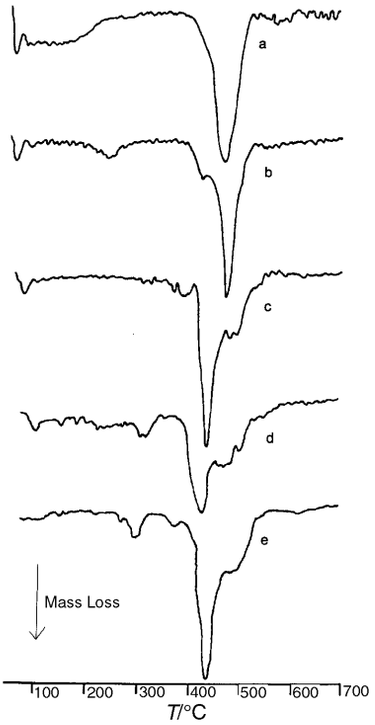

Fig. 5 DTG traces for a) pure (Al)-ZSM-5; and x = b) 64, c) 320, d) 640 (Ru(VI)), and e) 320 (Ru(VII)) -substituted ZSM-5 heated in flowing nitrogen from 40 °C to 700 °C at a rate of 20 °C min^{-1}.

Table 3 Percentage weight loss with increasing temperature (40–700 °C) for Al-MFI and Al(Ru)-MFI samples during thermogravimetric analysis, under flowing nitrogen

x	Peak range/°C	Peak maximum/°C	Mass loss (%)
0	400–500	468	13.46
32	400–500	460	14.45
64	400–500	470	14.26
320	350–450	404	14.92
320 (Ru(VII))	350–450	425	15.98
640	350–450	413	14.09

reflect the lower attraction to polar water molecules of Ru^{3+} over Al^{3+} due to a lower charge : radius ratio.

The increased complexity and peak shifts of the 350–550 °C region are due to changes in the type and number of TPA species present as a result of decreasing Al^{3+}/increasing Ru^{x+} content. In this region, there are three recognised thermal events reported for TPA-(Al)ZSM-5: a weak, broad shoulder at ~300 °C corresponding to the decomposition of TPA^+ associated with 'defect' ≡Si–O^- groups at the crystal surface; a strong endothermal peak at 390 °C, together with two shoulders at 420 °C and 450 °C, due to the 4-stage decomposition of ion-paired TPA^+OH^-; and a strong endothermal peak at 470 °C due to decomposition of charge-compensation TPA^+.[13,14] The 'shoulder' occurring at approximately 400 °C in (Al)ZSM-5 becomes more defined and more intense with increasing ruthenium substitution, the maximum weight loss moving from 460 °C to approximately 415 °C. At the same time the 435–530 °C region becomes less intense, and more asymmetric/broad.

The increasing intensity of the 415 °C peak may be due to charge-balancing TPA^+ ions allied to the presence of an increasing number of tetrahedral Ru^{3+} centres, but with an overall weaker association than observed for framework aluminium. However, owing to the increased complexity and reduced intensity of the higher temperature region, with increasing aluminium replacement by ruthenium, it is more likely that an overall reduction in the number of TPA^+ species required for charge compensation, and increase in the number of TPA^+OH^- species, has occurred. This change in thermal behaviour has been observed by Soulard *et al.*[13] in moving from (Al)-ZSM-5 to Silicalite®. This would imply that the ruthenium present (framework or extra-framework) has an oxidation state greater than +3, and may be involved in the catalytic breakdown of ion-paired TPA. No noticeable changes in the thermal character of the ruthenium samples were observed on changing the sample gas to air or oxygen.

Direct quantitative determination of ruthenium cannot be carried out by X-Ray Fluorescence spectroscopy, due to interference between the main spectral lines for ruthenium and the rhodium lines of the spectrometer's (ARL 8410) X-ray tube. Semi-quantitative elemental analysis of crystalline material was therefore carried out using Energy Dispersive X-Ray analysis. Unit-cell compositions are given in Table 4. Although ruthenium was not detected by EDX in the lower-substituted samples, the metal was detected, qualitatively, by

Table 4 Unit-cell composition of crystalline samples by semi-quantitative EDX and TGA/DTG analysis

	Number of atoms per unit cell							
x	Si	Al	Ru	K	TPA	[K + TPA]	O	H_2O/ molecules
0	81.62	15.10	—	9.30	2.90	12.20	18	21.5
32	81.08	15.73	—	8.67	3.79	12.46	18	18.46
64	88.38	7.90	—	3.27	3.52	6.79	18	16.18
320	91.71	—	2.77	1.73	4.30	6.03	18	11.67
320 (Ru(VII))	85.57	—	8.68	2.29	4.70	6.99	18	14.06

XRF (Fig. 6). It must be noted that the EDX beam has a lower penetrative power than that of XRF, and that EDX is, relatively, a 'surface' technique. XRF confirms a steady increase in ruthenium content within the crystals, relative to that in the gel, and detection in the lower-substituted samples also provides a convincing argument for the coordination of ruthenium within the bulk crystalline framework. However, the enhanced ruthenium content of the $x=320$ substituted Ru-ZSM-5 (Ru(VII)), when compared to the silica content, suggests further evidence for the presence of significant amounts of occluded and extra-framework ruthenium.

The difficulty of incorporation of aluminium within the framework of ZSM-5 is well known, and indeed, it has been suggested that the nucleation/crystallisation mechanism proceeds *via* Silicalite (pure-Si zeolite).[15] These literature observations, coupled with general reports of the low reactivity of ruthenium with non-metals, might account for the trend of increasing Si content with increased Al replacement by ruthenium. There is an overall decrease in the amount of K^+, $[K^+ + TPA^+]$, and a very slight increase in the amount of TPA^+ detected, with increased ruthenium in the gel. It has been suggested that metal cations and TPA^+ 'compete' for access to the zeolite channels, and that the amount of TPA^+ lost at higher temperatures (see TGA/DTG results) may be directly correlated to the amount of Al incorporated into the framework.[14] This same trend (and similar values) has been reported for ZSM-5, on reduction of Al levels.[13] However, the general reduction in 'charge-balancing' cations again suggests the presence of ruthenium in a greater oxidation state than +3.

X-Ray Photoelectron Spectroscopy was carried out on selected samples in an attempt to determine the oxidation state of ruthenium in the substituted zeolites. Ruthenium fairly readily adopts tetrahedral coordination, and forms stable oxo species in both oxidation states IV and VI. Therefore, when incorporated into a zeolite framework, the metal may possibly adopt either oxidation state. However, any traces of un-bound, occluded ruthenium are likely to be in the form of ruthenium(IV) oxide, as this is the most stable oxide. The most sensitive ruthenium XPS levels are the $3d_{5/2}$ and the $3d_{3/2}$ peaks. However, this 3d doublet almost coincides, in binding energy, with the C1s level,[16] and although the $3d_{5/2}$ and $3d_{3/2}$ were clearly detectable in the RuO_2 standard (281.8 eV and ~285 eV respectively), they were largely obscured by signals from residual template, even in the calcined forms. For this reason, the slightly less-sensitive Ru3p level was used to determine the oxidation state of ruthenium.

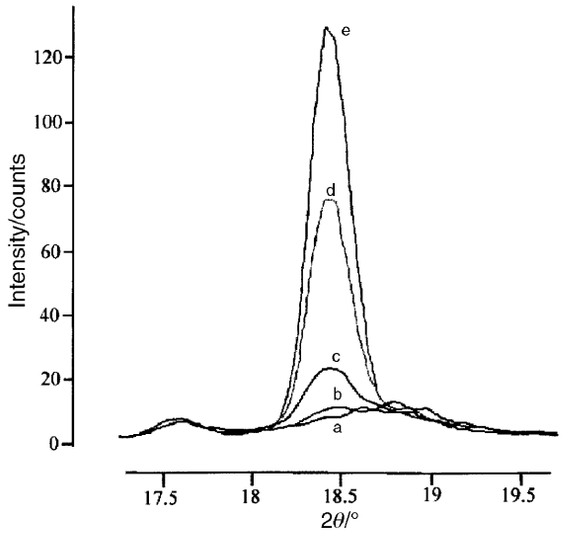

Fig. 6 Qualitative analysis of ruthenium by XRF—Ru-$K\alpha_{1,2}$ for a) Al-ZSM-5; and x = b) 32, c) 64, d) 320 and e) 640 ruthenium-substituted ZSM-5 (Ru(VI)).

The $Ru3p_{3/2}$ level in the RuO_2 standard occurred at 463.6 eV. For the $x=64$ Ru-ZSM-5 sample, the Ru3p level was barely detected, and no $Ru3d_{5/2}$ level was observed. The latter may be due to very low intensity, or the signal may be hidden under the C1s level (as previously stated). A very weak intensity $Ru3p_{3/2}$ level, having a binding energy of ~462 eV, *i.e.* below that of Ru(IV) oxide, was detected. No binding energy levels above this were observed. The Ru3p levels were again barely detectable in the $x=320$ Ru-ZSM-5 sample (as K_2RuO_4). However, close examination detected two levels at 462.8 eV and 467 eV. The former is likely to be due to traces of Ru(IV), but the latter, together with an $Ru3d_{5/2}$ level at 280.8 eV, *i.e.* below the value of 282 eV for Ru(IV), but above the binding energy for Ru(0) of ~280 eV,[16] may be due to a higher oxidation state of ruthenium than +4. The Ru3p levels of the $x=640$ Ru-ZSM-5 (as K_2RuO_4) sample were clearly detected, along with a $Ru3d_{5/2}$ level at 281 eV. Again the possible presence of two ruthenium states at 463 eV and 467 eV was observed.

As no literature data are available for the variation of Ru3p binding energy with oxidation state, then data have to be extrapolated from $Ru3d_{5/2}$ levels. Literature values for Ru(0) have $Ru3d_{5/2}$ levels at 280.0 eV[16] and Ru(IV) at 280.9 eV.[16] Similar data for $BaRuO_4$ show an $Ru3d_{5/2}$ level at 284.2 eV. In this work, shifts in the Ru3p level of 4 eV have been detected, it is therefore likely that the majority of the ruthenium present in the $x=320$ and 640 Ru-ZSM-5 samples is incorporated into the framework and in oxidation state +6 (467 eV), and that the weak 462 eV signals may be due to coordinated +4 ruthenium. As the zeolites tested were the original calcined forms, *i.e.* before modification to heating in an inert atmosphere, the slight traces of ruthenium with binding energy 463 eV may be assigned to particles of ruthenium(VI) oxide.

Conclusion

Using basic, tetrahedral RuO_4^{2-}, ruthenium-substituted MFI-type zeolite has been prepared with up to twice the mole fraction Al_2O_3 replaced by Ru_2O_3 in the gel. All crystalline products were white/grey in colour, indicating the presence of only tiny quantities of occluded oxides, and the mother liquors were light orange. Evidence for lattice incorporation was obtained from XRD. All samples, Al-MFI and Ru-MFI, showed excellent pattern matching to ICDD [38-195]. Increased Al^{3+} replacement resulted in a notable peak shift: increased *d*-spacings; and changes in the unit-cell parameters were observed, reflecting the larger size of the ruthenium ion. XPS data indicate two oxidation states for ruthenium. The majority of the metal appears to be incorporated into the framework and in oxidation state +6 (467 eV). However, the weak 462 eV signals, and the slight traces of ruthenium with binding energy 463 eV may be due to coordinated +4 ruthenium, and particles of ruthenium(VI) oxide, respectively.

Although crystalline MFI-type material was isolated from gels containing TPA perruthenate(VII), their dark colour, thermal instability and chemical analysis suggest that if Ru is taken into the framework, it is only loosely held, and that the structure readily collapses on heating to give finely dispersed ruthenium(VI) oxide within the annealed silicate.

Acknowledgements

The authors would like to thank J. A. Busby for XPS data, and Johnson Matthey for their financial support.

References

1 C. T. Chu and C. D. Chang, *J. Phys. Chem.*, 1985, **89**, 1569; J. Dwyer and P. J. O'Malley, *Stud. Surf. Sci. Catal.*, 1987, **35**, 219; R. B. Borade, *Zeolites*, 1987, **7**, 398.

2 C. S. John, D. M. Clark and I. E. Maxwell, *Perspective in Catalysis*, ed. J. M. Thomas and K. I. Zamaroev, Blackwell Science, Oxford, 1991, p. 387; W. F. Holderich, M. Hesse and F. Naumann, *Angew. Chem., Int. Ed. Engl.*, 1988, **27**, 226; B. Delmon, *Catal. Lett.*, 1993, **22**(1–2), 1.
3 M. Breysse, M. Cattenot, V. Kougionas, J. C. Lavalley, F. Mauge, J. L. Portefaix and J. L. Zotin, *J. Catal.*, 1997, **168**(2), 143; S. K. Das and P. K. Dutta, *Microporous Mesoporous Mater.*, 1998, **22**(1–3), 475; P. K. Dutta, *J. Incl. Phenom. Mol. Recogit. Chem.*, 1995, **21**(1–4), 215.
4 Y. F. Chang, J. G. McCarthy and E. D. Wachsman, *Appl. Catal. B: Environ.*, 1995, **6**(1), 21; V. I. Parvulescu, V. Parvulescu, S. Coman, C. Radu, D. Macovei, R. Angelescu and R. Russu, *Catal. Lett.*, 1995, **91**, 561.
5 C. T. Fishel, R. J. Davis and J. M. Garces, *J. Catal.*, 1996, **163**(1), 148; R. Carli, C. L. Bianchi and V. Ragaini, *Catal. Lett.*, 1995, **33**(1–2), 49.
6 W. P. Griffith, S. V. Ley, G. P. Whitcombe and A. D. White, *J. Chem. Soc., Chem. Commun.*, 1987, 1625.
7 G. Green, W. P. Griffith, D. M. Hollinshead, S. V. Ley and M. Schröder, *J. Chem. Soc., Perkin Trans. 1*, 1984, 681.
8 M. G. Howden, CSIR Report CENG 413, CSIR, Pretoria, 1982.
9 J. P. Verduijn, *Int. Pat.* WO92/13799, 1992 (Exxon Chemicals).
10 E. M. Flanigen, H. Khatami and H. A. Szymanski, *Molecular Sieve Zeolites*, *Adv. Chem. Ser.*, American Chemical Society, Washington DC, 1971, **vol. 101**, pp. 201–229.
11 G. Ricchiardi and J. M. Newsam, *J. Phys. Chem. B*, 1997, **101**(48), 9943.
12 E. de Vos Burchart, J. C. Jansen, B. van der Graaf and H. van Bekkum, *Zeolites*, 1993, **13**, 216.
13 M. Soulard, S. Bilger, H. Kessler and J. L. Guth, *Zeolites*, 1987, **7**, 463.
14 J. El Hage-Al Asswad, N. Dewaele, J. B. Nagy, R. A. Hubert, Z. Gabelica, E. G. Derouane, F. Crea, R. Aiello and A. Nastro, *Zeolites*, 1988, **8**, 221.
15 M. Padovan, G. Leofanti, M. Solari and E. Moretti, *Zeolites*, 1984, **5**, 295.
16 S. P. Sheu, H. G. Karge and R. Schlögl, *J. Catal.*, 1997, **168**(2), 278.